J Mater Sci: Mater Electron (2012) 23:1728–1733
DOI 10.1007/s10854-012-0654-4

Effect of CaO-doped in $NiMn_2O_4$–$LaMnO_3$ composite ceramics on microstructure and electrical properties

Fang Guan · Huimin Zhang · Aimin Chang · Pengjun Zhao · Bo Zhang

Received: 27 December 2011 / Accepted: 8 February 2012 / Published online: 21 February 2012

Abstract The composite ceramics $(NiMn_2O_4)_{0.50}(La_{1-x}Ca_xMnO_3)_{0.50}$ $(0 \leq x \leq 0.3)$ consisting of spinel-structured $NiMn_2O_4$ and perovskite-structured CaO-doped $LaMnO_3$ were prepared by classical solid state reaction. The X-ray diffraction (XRD) patterns have shown that the major phases presented in the sintered samples are $NiMn_2O_4$ compounds with a spinel structure, $La_{1-x}Ca_xMnO_3$ with a perovskite structure. The Scanning Electron Microscope (SEM) pictures have exhibited that the grain size of the composite ceramics decreases from ca. 6.5 to 2.0 μm as the mole fraction of CaO increases from 0 to 0.3. The $\rho_{25\ ^\circ C}$ and $B_{25/50}$ constants of the composite samples are in the range of 0.234–8.61 Ω cm and 2,600–2,962 K, respectively. In particular, CaO-doped leads to a decrease in the resistance drift of the $(NiMn_2O_4)_{0.50}(La_{1-x}Ca_xMnO_3)_{0.50}$ composite NTC (negative temperature coefficient) ceramics after aging test. This indicates that the CaO-doped $(NiMn_2O_4)_{0.50}$ $(La_{1-x}Ca_xMnO_3)_{0.50}$ NTC ceramics display high electrical stability in comparison with the Ca-free $(NiMn_2O_4)_{0.50}$ $(LaMnO_3)_{0.50}$ ceramics. The X-ray photoelectron spectroscopy (XPS) analysis verifies that the valence states of the manganese ions have a highly mixed state of Mn^{2+}, Mn^{3+} and Mn^{4+} at B site. And the electrical conduction of the composite ceramics can be elaborated by the ions migration mechanism.

F. Guan · H. Zhang · A. Chang (✉) · P. Zhao · B. Zhang
Xinjiang Key Laboratory of Electronic Information Materials and Devices, Xinjiang Technical Institute of Physics and Chemistry, CAS, Urumqi 830011, People's Republic of China
e-mail: changam@ms.xjb.ac.cn

F. Guan · P. Zhao · B. Zhang
Graduate School of the Chinese Academy of Sciences, Beijing 100049, People's Republic of China

1 Introduction

The NTC thermistors (TRs) based on mixed transition-metal and rare earth metal manganite electroceramics have been widely used for temperature measurement, control, compensation and suppression of inrush current, due to their high stability and low cost [1, 2]. In practice, the NTC thermistors are generally characterized by two parameters: B, the thermal constant which indicates a sensitivity to temperature excursions ($B = Ea/k$, unit in Kelvin, in which Ea is the electronic activation energy and k is the Boltzmann constant) and $\rho_{25\ ^\circ C}$, the resistivity at 25 °C. By compounding spinel and perovskite structure oxides, varying their relative proportions, doping with Alkalierdelement and controlling the processing conditions, a right combination of the resistivity and B value can be obtained [3].

The popular NTC materials are Ni- and Mn- based spinel oxides of general formula AB_2O_4, such as Mn–Ni–Co–O, Ni–Cu–Mn–O, Fe–Mn–Ni–O, Mn–Ni–Co–Zn–O [4–7]. For those spinel oxides, a high B value generally couples with high electrical resistivity and vice versa. However, some applications such as suppressing the inrush current require NTC materials with a low electrical resistivity (≤10 Ω cm) while possessing a large B (≥2,600 K) and sufficient stability. Therefore, there is a need for the development of new materials that have good electrical characteristics in suppressing the inrush current. Traditional methods to design a new material are composite and doping. Zhao et al. [8] have studied the composites made of spinel-structured $(Ni, Mn)_3O_4$ and perovskite-structured $La(Mn, Ni)O_3$, and found that the electrical resistivity of the composite decreased depending on the amount of the perovskite phase. Luo et al. [9] have prepared a composite ceramics material with high electrical resistivity and low B by introducing yttrium-stabilized zirconia as the second phase into

$Fe_{0.5}Cu_{0.2}Ni_{0.66}Mn_{1.64}O_4$ spinel matrix, the former is of high electrical resistivity and the latter of low electrical resistivity and low B. In principle, the material with low electrical resistivity and high B may be obtained through introducing a second phase with low electrical resistivity into a spinel oxide of high B. What's more, the composite can make full use of favorable condition and promote complementarity in each component due to the adjustability of its multiplicity and binding form [10], and the outstanding and attractive properties that the single component couldn't achieve may be obtained by complex method. Therefore, we propose an alternative approach by introducing a highly conductive component doped by a certain element into the spinel oxide. Perovskite structure $LaMnO_3$ is a good electronic conductor with the electrical resistivity of <than 1 Ω cm at 25 °C [11]. The Ca ion has a stable valence state bivalence and the Ca^{2+} has a approximate ionic radii with La^{3+}(the radius of Ca^{2+}, La^{3+} are 0.1000 and 0.1032 nm, respectively). Proper substitution of La for Ca may also decrease the resistivity of $LaMnO_3$ [12]. In the present work, the effects of CaO-doped in $NiMn_2O_4$–$LaMnO_3$ composite ceramics on microstructure and electrical properties are investigated.

2 Experimental procedure

The $NiMn_2O_4$ and $La_{1-x}Ca_xMnO_3$ ($0 \leq x \leq 0.3$) powder was synthesized using the conventional solid-state reaction method. The raw materials were analytical reagent La_2O_3, CaO, MnO_2 and Ni_2O_3. With appropriate amounts of those oxides, $NiMn_2O_4$ and $La_{1-x}Ca_xMnO_3$ powder was ball-milled at room temperature for 8 h separately in agate containers using agate balls as the milling medium and deionized water as a dispersant. The two kinds of ball milled slurry were then dried at 80 °C and calcined for 2 h at 1,000 °C respectively. The powder was ball-milled for 8 h again to break agglomerates.

With a mass ratio of the as-prepared $NiMn_2O_4$ powder to $La_{1-x}Ca_xMnO_3$ powder of 1:1, the mixture was grinded and then sieved. Disk-shaped compacts with a diameter of 10 mm and a thickness of 2 mm were formed by uniaxial pressing the powder at 60 MPa followed by isostatic cool pressing at 350 MPa. These green compacts were sintered at 1,300 °C for 4 h under air atmosphere.

The phase composition of the composite was determined by X-ray diffraction (XRD: BRUKER D8-ADVANCE, Germany) with Cu $K\alpha$ radiation ($\lambda = 1.5406$ Å). The microstructure and element compositions of sintered samples were observed by the Scanning Electron Microscope (SEM; LEO1430VP, Germany) in combination with energy dispersive spectroscopy (EDS; OXFORD INCA200, England). The X-ray photoelectron spectroscopy (XPS: Kratos Amicus, England) analysis was performed on the compacts in an ultrahigh vacuum and the spectra were recorded using an Mg $K\alpha$ X-ray source ($hv = 1{,}256.6$ eV). For electrical properties measurements, two opposite sides of the sintered compacts were coated with silver-palladium conductive paste, heated at 835 °C for metallization. The resistances of the composite were measured with disk-shaped samples using the Agilent 34401A digital multimeter. To ensure the temperature deviation from the designated value to be <±0.05 °C, samples were immersed in silicon oil. The thermal constant B was calculated according to the formula $B = 3{,}853.89 \cdot \ln (R_{25}/R_{50})$, in which R_{25} and R_{50} are the resistances at 25 and 50 °C, respectively. To obtain aging properties, these samples were aged by heat treatment at 125 °C in air for 500 h, and the aging is characterized by $\Delta R/R_0 = (R - R_0)/R_0$, in which R_0 and R are the resistivity at 25 °C before and after the heat treatment.

3 Results and discussions

3.1 Phase composition and microstructure

Figure 1 shows the XRD patterns of $NiMn_2O_4$ $(NiMn_2O_4)_{0.50}$ $(La_{1-x}Ca_xMnO_3)_{0.50}(0 \leq x \leq 0.3)$ and $La_{0.9}Ca_{0.1}MnO_3$ samples sintered at 1,300 °C. It can be seen that the composite ceramics are consisted of cubic structure spinel phase and orthorhombic structure perovskite phase. Before compositing, there is a little amount of monoclinic structure rock-salt NiO phase separated out from the spinel phase $NiMn_2O_4$ matrix and then disappeared in composites. It may be that introducing $LaMnO_3$ doped by CaO into $NiMn_2O_4$ retarded the separating process of rock-salt NiO phase. In addition, the substitution of La for Ca doesn't change the perovskite structure of $LaMnO_3$. Compared to the single phase without compounding, the interplanar

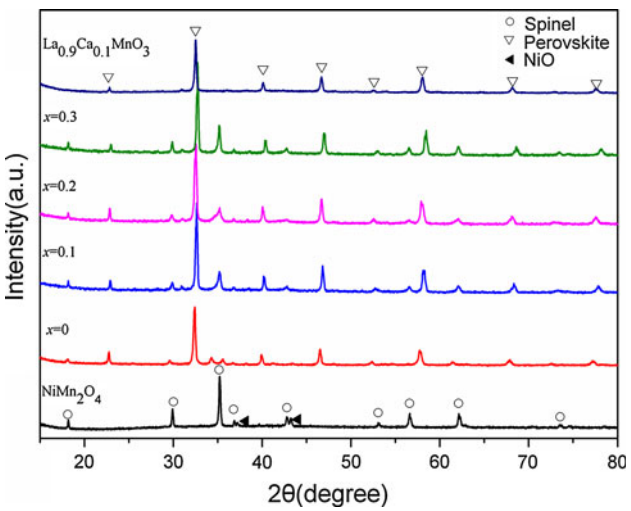

Fig. 1 The XRD patterns of $NiMn_2O_4$, composites of $(NiMn_2O_4)_{0.50}$ $(La_{1-x}Ca_xMnO_3)_{0.50}$ ($x = 0$, 0.1, 0.2, 0.3) and $La_{0.9}Ca_{0.1}MnO_3$

Table 1 The effective ionic radii of different ions with different coordination numbers

Coordination number	Ionic radii (nm)					
	La^{3+}	Ca^{2+}	Ni^{2+}	Mn^{2+}	Mn^{3+}	Mn^{4+}
4	–	–	0.0550	0.0660	–	0.0390
6	0.1032	0.1000	0.0690	0.0830	0.0645	0.0530
12	0.1360	0.1340	–	0.0900	–	–

spacing of (111) in the spinel phase increases from 4.8561 to 4.8704 Å, while the interplanar spacing of (101) in the perovskite phase decreases from 3.8914 to 3.8824 Å in $(NiMn_2O_4)_{0.50}$ $(La_{0.9}Ca_{0.1}MnO_3)_{0.50}$ sample.

The observed changes of the interplanar spacing can be explained in terms of valence and size of the cations occupying the octahedral sites. The Mn-rich spinel induced by the separation of the NiO is known to possess a cationic distribution $[Mn^{2+}]\left[Ni_{\alpha}^{2+}Mn_{2-2\alpha}^{3+}Mn_{\alpha}^{4+}\right]O_4$ [13]. According to this result, when a Ni^{2+} ion is replaced by a Mn^{3+} ion, to maintain the electrical neutrality of the lattice, a Mn^{4+} ion has to convert to Mn^{3+}. In other words, annihilation of one Ni^{2+} ion is accompanied by the annihilation of one Mn^{4+} ion and generation of two Mn^{3+} ions. Accordingly, the sum of these two Mn^{3+} ions in size is larger than that of one Ni^{2+} ion and one Mn^{4+} ion based on Table 1 [14], and it explains the larger interplanar spacing observed from the Mn-rich spinel phase. As to the perovskite phase, both the migration of Ni^{2+} ions and the substitution of Ca^{2+} for La^{3+} make the change of ions valence state toward the opposite direction. The Mn^{3+} at B site in the perovskite structure is replaced by Ni^{2+} and this process leads to annihilation of two Mn^{3+} ions accompanying by generation of one Ni^{3+} ion and one Mn^{4+} ion which induces decrease of the interplanar spacing. Moreover, the radius of Ca^{2+} is smaller than La^{3+} and then the substitution of Ca^{2+} for La^{3+} also results in the decrease in the interplanar spacing of the perovskite phase.

Figure 2 shows the SEM images of the composite samples $(NiMn_2O_4)_{0.50}(La_{1-x}Ca_xMnO_3)_{0.50}$ sintered at 1,300 °C. From these SEM figures, it is immediately seen that the average grain size decreases from 6.5 to 2.0 μm with x increasing from 0 to 0.3, crystalline grains become integrated and uniform and the grain boundary turns more distinguishable. Obviously, the presence of the perovskite phase doped by CaO suppresses the grain growth and produces great influence on the microstructure of the composites. It is known that La can scatter electrons much more effectively than Mn, Ni and Ca, for the atomic number of the former is much larger than those of the latter. A reasonable conclusion can be drawn that the brighter area corresponds to the perovskite phase, while the darker area the spinel phase which is verified by the EDS spectra in Fig. 3. Based on the SEM/EDS results, Table 2 shows the values of weight and atomic percentages obtained from different spots in Fig. 2a4. The EDS spectra of spot A refers to the brighter area where is La-rich and Ni-poor area, while the EDS spectra of spot B referring to darker area is the contrary. From Table 2, it also can be seen that there is no pure $La_{1-x}Ca_xMnO_3$ or $NiMn_2O_4$ existed in the sintered body, which may indicate that the perovskite phase and the spinel phase formed solid solution during sintering process and ions migration occurred between two phases.

3.2 Electrical properties

Figure 4 shows the Arrhenius plot of the resistivity of the composites in the temperature ranging from −35 to 50 °C. It can be seen that the composites exhibit typical NTC effect. Thermal constant B and $\rho_{25\ ^\circ C}$ of $(NiMn_2O_4)_{0.50}$ $(La_{1-x}Ca_xMnO_3)_{0.50}$ as a function of doping CaO content are presented in Fig. 5. The resistivity of the composites first decreases and then increases as x value increases from 0 to 0.3. When $x = 0.3$, the value of resistivity is even larger than the CaO-free samples. In contrast, the thermal constant B increases sharply from 1,639 to 2,962 K with x increasing from 0 to 0.3. Therefore, a small quantity ($\leq$0.2) of CaO-doped can produce a composite which possessed a right combination of resistivity and thermal constant ($\rho_{25\ ^\circ C} \leq 8.61\ \Omega$ cm, $B \geq 2{,}690$ K) required for the application of suppressing the inrush current. The aging coefficient ($\Delta R/R_0$) for the composites is shown in Fig. 6. It can be seen that the values of $\Delta R/R_0$ decreases with an increase in x. For $x = 0.3$, the resistivity of the composite was increased by 0.34% after aging at 125 °C in air for 500 h, while 5.02% for the samples without doping CaO. It is likely that the presence of CaO provides a physical barrier to the aging of the composite [15].

As to the electrical conduction of the composite ceramics, it can be explained well by the ions migration mechanism and the ions migration mainly happens at B sites between the spinel structure $NiMn_2O_4$ and perovskite structure $La_{1-x}Ca_xMnO_3$ as the followed Eq. 1.

$$\begin{aligned} La_{1-x}Ca_xMnO_3 + Ni_{1-a}Mn_a[Ni_aMn_{2-a}]O_4 \\ \rightarrow La_{1-x}Ca_x[Mn_{1-b}Ni_b]O_3 \\ + \ Ni_{1-a}Mn_a[Ni_{a-b}Mn_{2-a+b}]O_4 \end{aligned} \quad (1)$$

The electrical conduction of the composite is mainly determined by the amount of the carriers and their mobility,

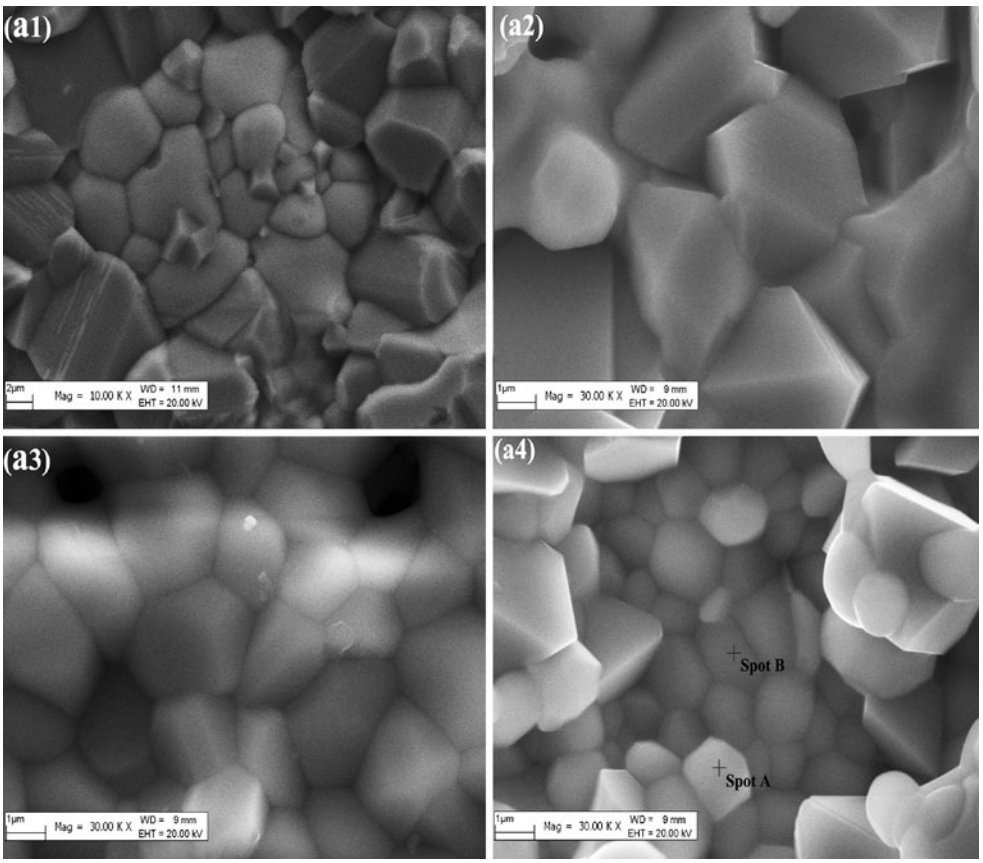

Fig. 2 SEM images of $(NiMn_2O_4)_{0.50}(La_{1-x}Ca_xMnO_3)_{0.50}$ with $x = 0$ $La_{1-x}Ca_xMnO_3$ (**a1**), 0.1(**a2**), 0.2(**a3**), 0.3(**a4**) sintered at 1,300 °C

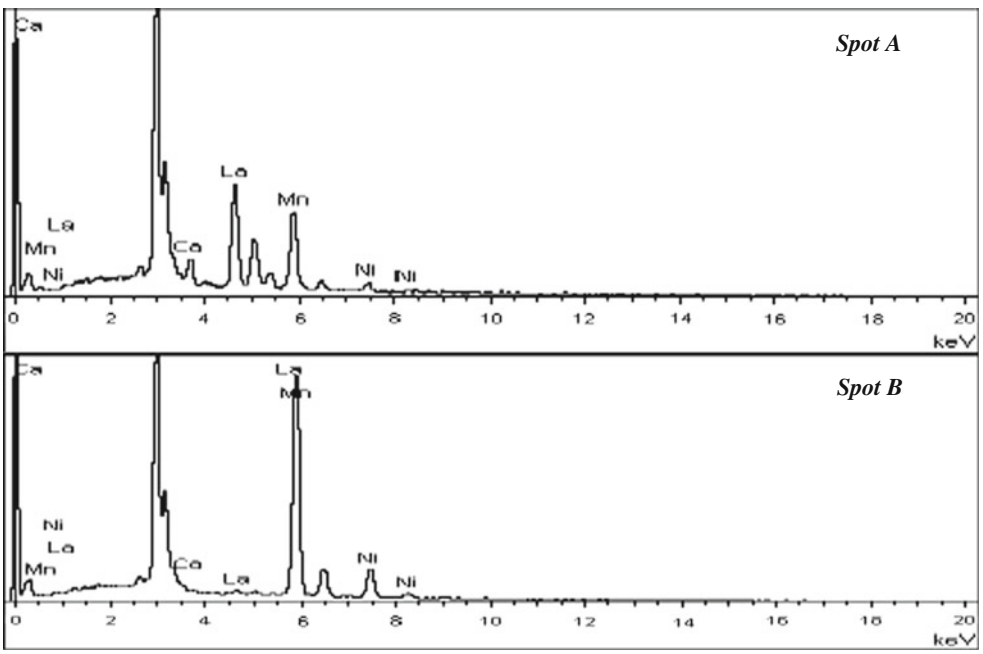

Fig. 3 Representative EDS spectra of different spots in Fig. 2a4

Table 2 Values of weight and atomic percentages obtained from different spots in Fig. 2a4

Spots	Line	Weight (%)	Atomic (%)
A	Ca K	3.85	8.29
	Mn K	29.97	47.08
	Ni K	4.12	6.06
	La L	62.06	38.57
B	Ca K	0.08	0.12
	Mn K	77.79	79.41
	Ni K	19.20	18.34
	La K	2.33	0.94

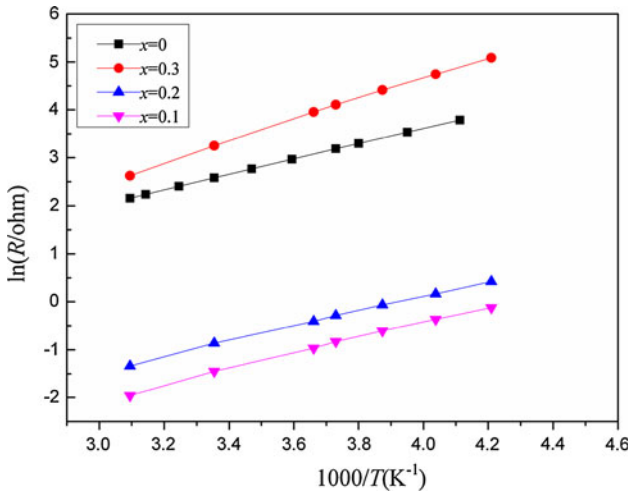

Fig. 4 Arrhenius *plot* of resistivity for $(NiMn_2O_4)_{0.50}(La_{1-x}Ca_xMnO_3)_{0.50}$

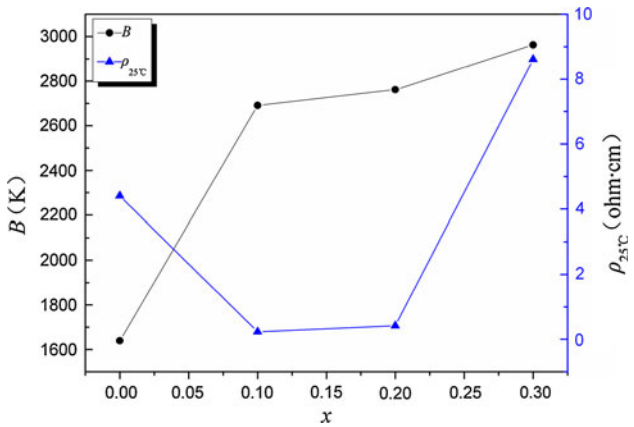

Fig. 5 Thermal constant B and $\rho_{25\ ^\circ C}$ of $(NiMn_2O_4)_{0.50}(La_{1-x}Ca_xMnO_3)_{0.50}$ as a function of mole fraction of the doped CaO x

especially for manganite, the ion pairs of different valence states, Mn^{3+}/Mn^{4+}, for example, influence the electronic transport behavior markedly [16]. CaO-doped changes the ratio of Mn^{3+}/Mn^{4+} in $LaMnO_3$ which effects the ion migration in the composite ceramics. The relationship

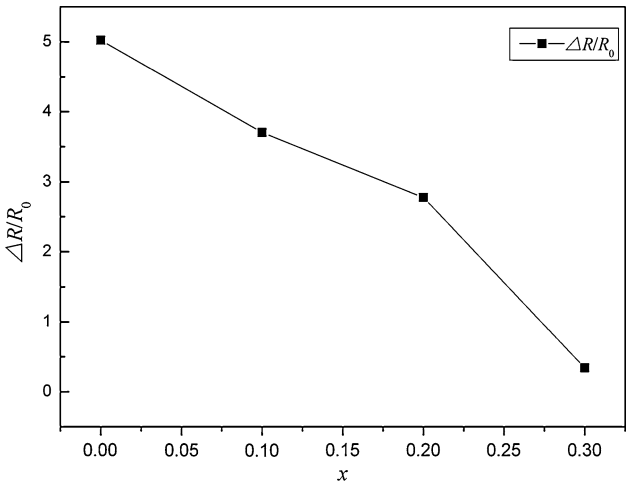

Fig. 6 Aging coefficient $\Delta R/R_0$ versus x for the $(NiMn_2O_4)_{0.50}(La_{1-x}Ca_xMnO_3)_{0.50}$ composites

between resistivity and x value in the composite ceramics can be explained as follows. For undoped $LaMnO_3$ where all the Mn ions are nominally in the tervalence state, predominant carriers are holes at room temperature. When La^{3+} is substituted by a small amount of Ca^{2+}, some of the Mn^{3+} ions shift their valence state from tervalence to tetravalence, which contributes to the enhancement of hole concentration. Consequently, the drop in the resistivity of $x = 0.1$ composite sample is considered to be associated with the increase of the hole concentration in the perovskite phase. Due to the radius of Ca^{2+} is a little smaller than La^{3+}, the increase of x induces the enhancement of lattice distortion and further decreases of interplanar spacing, which bates the Ni^{2+} ions migration between two phases because it also reduces the interplanar spacing of the perovskite structure $La_{1-x}Ca_xMnO_3$ with $x = 0.2$, 0.3.

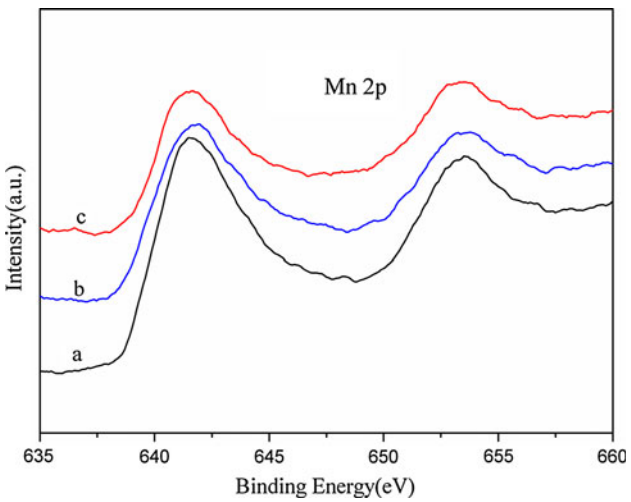

Fig. 7 The Mn 2p spectra for $NiMn_2O_4$ (*a*), $La_{0.9}Ca_{0.1}MnO_3$ (*b*) and $(NiMn_2O_4)_{0.50}(La_{0.9}Ca_{0.1}MnO_3)_{0.50}$(*c*)

Table 3 The binding energy and paek intensity of Mn $2p_{3/2}$ obtained from the XPS spectrum

Sample	Mn $2p_{3/2}$ binding energy (eV)			Mn $2p_{3/2}$ peak intensity (%)		
	Mn^{2+}	Mn^{3+}	Mn^{4+}	Mn^{2+}	Mn^{3+}	Mn^{4+}
$NiMn_2O_4$	640.4	641.6	643.1	34.84	31.91	33.25
$La_{0.9}Ca_{0.1}MnO_3$	637.1	641.5	644.6	31.78	41.83	26.39
$(NiMn_2O_4)_{0.50}(La_{0.9}Ca_{0.1}MnO_3)_{0.50}$	640.2	641.4	642.8	32.31	27.09	40.60

Therefore, the ion pair number of different valence states (Mn^{2+}/Mn^{3+}, Mn^{3+}/Mn^{4+}) decrease, then the electrical conduction of the composite weakens. Therefore, as the amount of CaO increases, the resistivity of the composite ceramics decreases to a minimum value and then increases, which is shown in Fig. 4.

The change of the composite electrical conductivity above can be confirmed further by the XPS results. Figure 7 shows the XPS spectra for the Mn 2p level of the samples $NiMn_2O_4$, $La_{0.9}Ca_{0.1}MnO_3$ and $(NiMn_2O_4)_{0.50}(La_{0.9}Ca_{0.1}MnO_3)_{0.50}$. In Table 3 it is summarized the binding energy and peak intensity value obtained from the XPS experiments using the approximate relationship: $\frac{n_1}{n_2} = \frac{I_1}{I_2} \cdot \frac{\sigma_1}{\sigma_2} \left[\frac{Ek_2}{Ek_1}\right]^{\frac{1}{2}}$ where n_1, Ek_1, and σ_1 are the number of atoms of element I, the kinetic energy value corresponding to the line considered, and the cross-section calculated theoretically, respectively[17]. From Fig. 6 and Table 3, it can be seen that the valence states of the manganese ions have a highly mixed state of Mn^{2+}, Mn^{3+} and Mn^{4+} at B site. Before compositing, the substitution of Ca^{2+} for La^{3+} in $LaMnO_3$ leads to the Mn^{3+} ions translating into Mn^{4+}, which produces more ion pair Mn^{3+}/Mn^{4+} and contribution to the high conductivity of the perovskite structure [16]. In the composite, in order to keep charge conservation, the migration of Ni^{2+} ions between two phases results in Mn^{4+} ions translating into Mn^{3+} in the spinel phase and Mn^{3+} ions translating into Mn^{4+} in the perovskite phase, and the latter is predominant which is in good agreement with the previously analysis and the peak intensity data in Table 3.

4 Conclusion

The composite ceramics $(NiMn_2O_4)_{0.50}(La_{1-x}Ca_xMnO_3)_{0.50}$ ($x = 0$, 0.1, 0.2, 0.3) consisted of spinel structure $NiMn_2O_4$ and perovskite structure $La_{1-x}Ca_xMnO_3$ were prepared by the conventional solid state reaction. Introduction of low-resistivity perovskite CaO-doped $LaMnO_3$ into the spinel oxide $NiMn_2O_4$ results in a decrease of the grain size from 6.5 to 2.0 μm, a large increase in B from 1,639 to 2,962 K as x increases from 0 to 0.3. The resistivity firstly decreases slightly with increasing CaO content from $x = 0$ to 0.1, and then in the range of $x \geq 0.1$, the resistivity increases as the amount of Ca content increases, however, the $\rho_{25\ ^\circ C}$ is always <8.61 Ω cm. Doping CaO in $LaMnO_3$ make the composite NTC thermistors have better electrical stability ($\Delta R/R_0 = 0.34\%$ when $x = 0.3$) in comparison with CaO-free thermistors ($\Delta R/R_0 = 5.02\%$ when $x = 0$). The electrical conduction of the two phase composite can be well described using the ion migration mechanism.

Acknowledgments The authors are thankful to the National Natural Science Foundation of China (Grant No. 50902148) and the "Western Light Joint Scholar Foundation" Program of Chinese Academy of Sciences (No. RCPY200901) for providing the financial support.

References

1. A. Feteira, J. Am. Ceram. Soc. **92**, 967 (2009)
2. M.M. Vakiv, O.I. Shpotyuk, V.O. Balitska, B. Butkiewicz, L.I. Shpotyuk, J. Eur. Ceram. Soc. **24**, 1243 (2004)
3. T. Yokoyama, T. Meguro, Y. Shimada, J. Tatami, K. Komeya, Y. Abe, J. Mater. Sci. **42**, 5860 (2007)
4. T. Yokoyama, T. Meguro, Y. Shimada, J. Tatami, K. Komeya, Y. Abe, J. Mater. Sci. **42**, 5860 (2007)
5. R.N. Jadhav, V. Puri, J. Alloy Compd. **507**, 151 (2010)
6. Z.B. Wang, C.H. Zhao, C.S. Chen, A.J.A. Winnubst, J. Eur. Ceram. Soc. **26**, 2833 (2006)
7. K. Park, J.K. Lee, S.J. Kim, W.S. Seo, W.S. Cho, C.W. Lee, S. Nahm, J. Alloy Compd. **467**, 310 (2009)
8. C.H. Zhao, Z.B. Wang, S.M. Wang, P.H. Yang, C.S. Chen, J. Electroceram. **20**, 113 (2008)
9. W. Luo, H.M. Yao, P.H. Yang, C.S. Chen, J. Am. Ceram. Soc. **92**, 2682 (2009)
10. M.L. Singla, S. Awasthi, A. Srivastava, D.V.S. Jain, Sens. Actuators A **136**, 604 (2007)
11. I. Maurin, P. Barboux, Y. Lassailly, J.P. Boilot, J. Solid State Chem. **160**, 123 (2001)
12. Z. Branković, K. Đuriš, A. Radojković, S. Bernik, Z. Jaglićić, M. Jagodić, K. Vojisavljevic, J. Sol–Gel Sci. Technol. **55**, 311 (2010)
13. S. Guillemet-Fritsch, J.L. Baudour, C. Chanel, F. Bouree, A. Rousset, Solid State Ion. **132**, 63 (2000)
14. R.D. Shannon, Acta Cryst. A **32**, 751 (1976)
15. K. Park, I.H. Han, J. Electroceram. **17**, 1079 (2006)
16. P.N. Lisboa-Filho, M. Bahout, P. Barahona, C. Moure, O. Pena, J. Phys. Chem. Solids **66**, 1206 (2005)
17. Y. Boudeville, F. Fiqueras, M. Forissier, J.L. Portefaix, J.C. Vedrine, J. Catal. **58**, 52 (1979)